Int J Adv Manuf Technol (2009) 40:1191–1201
DOI 10.1007/s00170-008-1424-6

ORIGINAL ARTICLE

Feedrate scheduling strategy for free-form surface machining through an integrated geometric and mechanistic model

Liqiang Zhang · Jingchun Feng · Yuhan Wang · Ming Chen

Received: 18 November 2007 / Accepted: 29 January 2008 / Published online: 13 March 2008

Abstract In free-form surface machining, it is essential to optimize the feedrate in order to improve the machining efficiency. Conservative constant feedrate values have been mostly used up to now since there was a lack of physical models and optimization tools for the machining processes. The overall goal of this research is the integration of geometric and mechanistic milling models for force prediction and feedrate scheduling in five-axis CNC free-form surface machining. For each tool move, the geometric model calculates the cut geometry, and a mechanistic model is used along with a maximum allowable cutting force to determine a desired feedrate. The results are written into the part NC program with optimized feedrates. When the integrated modeling approach based feedrate scheduling strategy introduced in this paper was used, it was shown that the machining time can be decreased significantly along the tool path.

Keywords Five-axis · Geometric simulation · Mechanistic model · Feedrate scheduling

1 Introduction

Free-form machining is one of the most commonly manufacturing processes used in various industries, such as aerospace and die mould industries. In planning process operations, the CAM program has to be conservative most of the time in selecting machining conditions in order to avoid undesirable results, such as cutter breakage or overcut. The production time and cost are the key factors in today's competitive market. However, conservative constant feedrate values have been mostly used to now, since there was a lack of physical models and optimization tools for the machining process. Currently the NC code generators are based on only the geometric and volumetric analysis, but not on the physical processes of the free-form machining yet. It is often difficult to select appropriate cutting conditions to achieve high productivity while maintaining part quality due to the complicated surface geometry. The selection of the feedrate must be performed carefully because excessive feedrate increase cutting forces, tool deflections and wears, etc. Therefore, a reliable force model based feedrate scheduling may provide a solution to solve this problem.

Feedrate scheduling for free-form surfaces has became popular recently. Two methods exist for conducting feedrate scheduling: one is based on the material removal rate (MRR) and the other is based on the cutting force. Many researchers have developed and used a feedrate scheduling system based on volumetric analysis by using material removal rate (MRR) approach. Lan [1] proposed a mathematical model and the decision criteria in order to achieve the optimal MRR control of a cutting tool. Li et al. [2] performed an offline feedrate optimization integrated with CAD/CAM by relating the average power with MRR.

Besides the MRR models, some researchers have performed off-line feedrate scheduling based on the mechanistic cutting force models. Yazar [3] performed feedrate optimization based on cutting force calculation in three-axis milling of dies and molds. Lim and Hsiang [4]

L. Zhang · J. Feng · M. Chen
School of Mechanical Engineering, Shanghai Jiaotong University, Shanghai 200240, People's Republic of China

Y. Wang (✉)
State Key Laboratory of Mechanical System and Vibration, Shanghai Jiaotong University, Shanghai, People's Republic of China
e-mail: yhwang@sjtu.edu.cn

proposed a cutting path adaptive feedrate strategy, which improves the productivity of free form surface machining when subjected to both force and dimensional constraints. Baek et al. [5] focused to find optimal feedrate for face milling operations in order to maximize MRR with a surface roughness constraints. Liu [6] presents an improved theoretical dynamic cutting force model for ball-end milling. Taunsi [7] integrated the feed drive dynamics with the minimum-time trajectory planning in order to achieve the desired feedrate at the appropriate position. Feng and Su [8] optimized the feedrate with the tool path based on the calculation of cutting forces and machining errors in 3D plane surface machining. Li [9] studied feedrate optimization for variant milling process based on cutting force prediction. Ko et al. [10] presented an off-line feedrate scheduling model based on the mechanistic cutting force model for flat end milling by adjusting the acceleration and deceleration time of the controller. Erdim et al. [11] built an off-line feedrate scheduling system for sculptured surface machining based on the cutting force model, which was built upon the previous studies of Guzel [12]. Li [13] built the framework of optimization system so that the processes of reliability verification, cutting parameter optimization and error compensation can be integrated into one system. Ko and Cho [14] proposed a scheme for off-line feedrate scheduling for 3D ball-end milling based on the cutting force model considering transverse rupture strength of the tool.

Present CAM technology does not consider important physical properties, such as cutting forces. Besides, some commercial software packages, such as Vericut's feedrate optimization module Optipath works on a volumetric analysis. They are based on the amount of material removal rate in each segment of the cut. The goal of this research is the integration of geometric and mechanistic milling models for sculptured surface machining force prediction and feedrate scheduling. The proposed strategy was tested under various cutting conditions and some of the results were presented in the paper.

2 Geometric model

2.1 Modeling of workpiece and toolpath representation

The geometric model performs two important functions in the feedrate selection process. It is responsible for providing the cut geometry for the mechanistic model, and it also serves as a dynamic geometric record for in-process workpiece. An accurate model is important to ensure that correct cut geometry parameters are calculated in the simulation process.

The method selected for geometric modeling in the paper is the extended dexel (depth element) approach. Compared to voxel model [15], which is used extensively in volume graphics, the advantage of using dexel volume model is its smaller memory requirement and fewer processing volume elements. Dexel volume model represents an object with a grid of long columns compacted together. In the dexel-updating process, each dexel is treated as a vector (Fig. 1). Material removal simulation is performed through calculation of intersections between these lines and a geometric representation of the swept toolpath envelope. The advantage of this approach is efficient rendering, as the stock model is the rendered model, and no additional processing is required. The drawback is that control over geometric accuracy is diminished, as it becomes a function of the stock size, number of screen pixels, and part orientation on the screen.

All in all, the dexel approach is very robust, requiring only simple line intersections performed between the stock and a model of the volume swept by a single tool move (swept toolpath envelop, or STE) to model material removal. The robust and efficient nature of dexel modeling

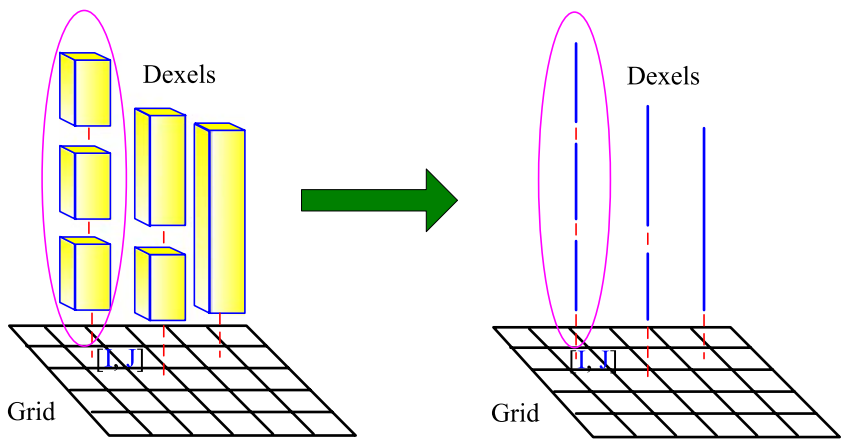

Fig. 1 The linked list data structure of dexel volume model

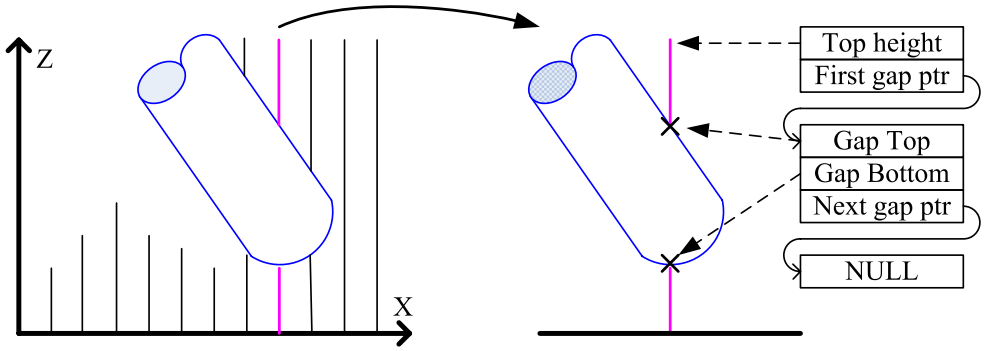

Fig. 2 Multiple intersections between toolpath envelope and dexel elements

has resulted in it becoming the leading method for commercial NC simulation software. In addition to the Vericut package by CGTech, there are other commercial implementations of dexel models. Each dexel element is composed of two components, a 'Top' value and a list of 'Gaps' (Fig. 2). The Top value represents the maximum height of the stock model at the location of that element. A 'gap' denotes a region in the element below the Top where a section of the dexel element is removed. Gaps consists of a gap top and a gap bottom, and also a pointer to the next gap in the list (if any). If there are no gaps present in an element, the Gap pointer defaults to null.

From a given pair of intersections between the dexel element and the STE, an 'intersected segment' is defined. The intersected segment defines the portion of dexel element that lies entirely within the STE, and represents the material removal contribution from that element. The entire intersected segment is known to contact the cutter, which simplifies the calculation of volumetric removal rate and contact area. The upper and lower ends of the intersected segment are initially set to the calculated upper and lower intersection locations. After this initial segment has been created, the ends of this segment are adjusted so that both are valid, defining the actual intersected segment. This is achieved by testing for three primary cases and several sub-cases: (1) The lower intersection lies above the top height of the element (Fig. 3): In this case the current element does not intersect the STE, and so no intersected segment is defined and the dexel element requires no updating. (2) The lower intersection lies below the top height, and the upper intersection lies above it (Fig. 4). In this common case, the upper end of the intersected segment is defined as the current element top height. The lower end is checked for validity and redefined to specify the final intersected segment. (2a) If the lower intersection is found to reside in a solid section of dexel, the definition of the ends of the intersected segment is completed by assigning its lower end the value of the lower intersection. (2b) If the lower intersection is found to reside in a gap, the definition of the ends of the intersected segment is completed by assigning its lower end the value of the gap top. (3) Both the upper and lower intersections lie below the top height (Fig. 5). In this case the two intersections either form a new gap or expand an existing gap in the element, which encompasses five sub-cases. (3a) If both the upper and lower intersections lie completely within a single existing gap, the current does not intersect the STE, and so no intersected segment is defined and the dexel element requires no updating. (3b) If neither the upper nor the lower intersections lie within an existing gap, the intersected segment is defined by assigning to its upper and lower ends the values of the upper and lower intersection locations respectively. (3c) If only the upper intersection lies within an existing gap, the intersected segment is

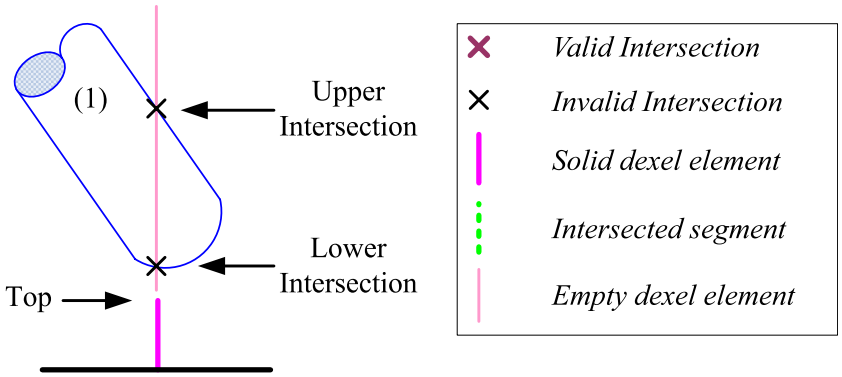

Fig. 3 The case 1 where no updating of the dexel model is required

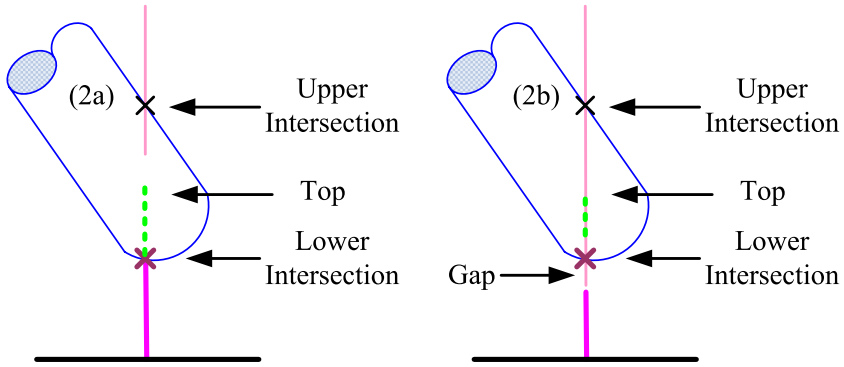

Fig. 4 The case two where either one or no valid intersections exist

defined by assigning to its upper end the value of gap bottom, and to its lower end the value of the lower intersection location. (3d) If only the lower intersection lies within and existing gap, the intersected segment is defined by assigning to its upper end the value of the gap top. (3e) If both the upper and lower intersections lie within separate existing gaps, the intersected segment is defined by assigning to its upper end the value of the upper gaps bottom, and to its lower end the value of lower gaps top.

The element is now completely updated, and then a contour display method [16] is used to generate contours that connect dexel faces (center points) along constant x and y grid address (Fig. 6). Thus two sets of equally spaced planar contours are displayed to represent dexel based objects. The contour points could be used to construct a triangular mesh for a smooth rendering of dexel based objects.

2.2 Calculation of geometric parameters

Following the intersection calculations for a given tool move, the cut geometry parameters are calculated. The cut geometry parameters define the region of the cutting tool engaged in the stock material for a given tool move. The contact area is of critical importance in determining the cutting forces because it describes the extent of tooth engagement for any cutter rotation position. The cutting edge model can be broken into a set of axial disc elements (Fig. 7). For each disc there are two primary geometric cut parameter concerns. The first concern is whether or not a given axial disc element is engaged in the stock. For a disc that is engaged in the stock, the second concern for discs engaged in the stock is to define the limits of engagement, defined in the mechanistic model via a set of entrance/exit angles (Fig. 8). The entrance and exit angles are calculated by solving for the normal direction component of each intersection, and storing the maximum and minimum normal positions found during a given tool move. The entrance and exit angles for up milling are found [17] using

$$\begin{aligned} \alpha_{entr} &= 1/\sin(D_{\max}/R) \\ \alpha_{exit} &= 1/\sin(D_{\min}/R) \end{aligned} \tag{1}$$

where R is the current axial disc radius. For down milling, the definitions of entrance and exit angles are reversed. Calculating D from intersection data is to calculate intersections between the dexel elements and each individual disc of the tool path envelope. In this approach, intersections are first calculated with the axially top-most disc element of the toolpath as if it were the entire toolpath, and the maximum and minimum D value, $D_{\max}$ and $D_{\min}$, are then calculated for that topmost disc. These values are calculated by defining a vector form the initial tool position, as defined in the NC program. By performing this dot with all intersections found with the disc, and storing the maximum and minimum values, $D_{\max}$ and $D_{\min}$

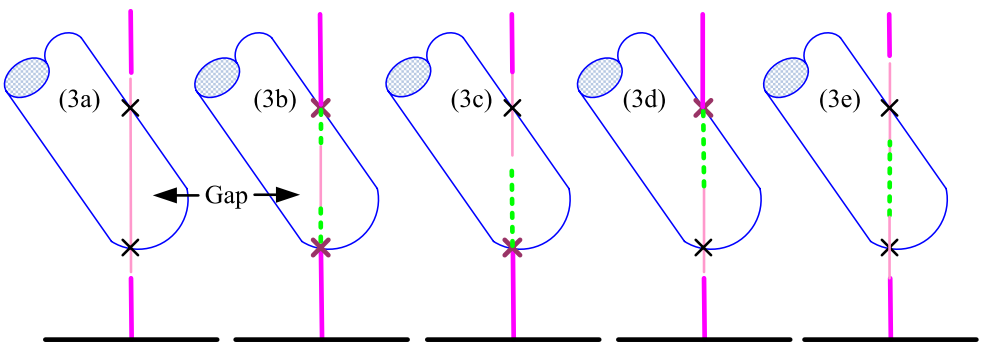

Fig. 5 The case three where both the upper and lower intersections lie below the top height

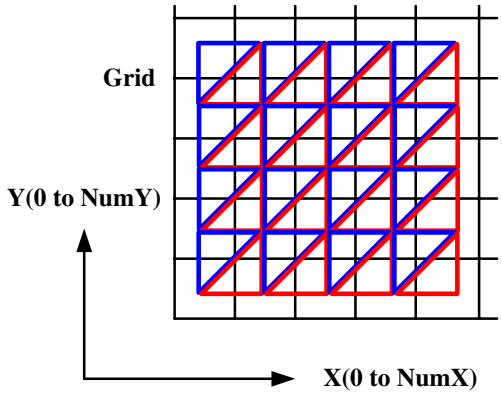

Fig. 6 Triangular meshes for the top and bottom surface

are found. The intersection is then stored in the dexel model, and this process is repeated for each subsequent axial disc element.

3 Modeling of cutting forces

3.1 Coordinate definitions and chip thickness model

The force model utilized in this research can be used to estimate forces for both flat and ball end milling. The force model needed to predict forces is discussed later, but first, the various coordinate systems used to characterize the tool and workpiece motion are defined along with the chip thickness.

Two sets of coordinates are used to describe the motion of the workpiece and tool in this paper. A workpiece coordinate system (WCS) with unit vector **i**, **j**, **k** is fixed to the workpiece, and a local tool coordinate system with unit vectors **u**, **v**, **w** is fixed to the end mill, with the origin at the ball center for a ball end mill, or the bottom radial center for a flat end mill. The CL file is usually expressed in terms of the WCS. This paper assumes that the tool paths are given in a CL file. If G-codes are to be simulated, they must be 'reverse post processed' to obtain tool motion in terms of the WCS.

The origin of the tool coordinate system is defined as the cutter location position of the initial tool position, in workpiece coordinates, denoted $\mathbf{P_i}$. There are four unit vectors used in the intersection calculations and to define the geometric cut parameters. The tool path unit vector **d** indicates the direction of travel of the cutting tool in workpiece coordinates during the current tool move. It is defined as

$$\mathbf{d} = (\mathbf{P}_f - \mathbf{P}_i)/|(\mathbf{P}_f - \mathbf{P}_i)| \tag{2}$$

where $\mathbf{P}_f$, $\mathbf{P}_i$ are the final and initial tool positions in workpiece coordinates respectively. The second unit vector corresponds to the tool axial direction z and is denoted **w**. This vector is determined from the cutter's orientation in workpiece coordinates, calculated for every tool path in the CL file.

The next unit vector, normal vector **v**, is orthogonal to **w** and **d** and defines the normal direction to the planar sides of the swept envelope in workpiece coordinates:

$$\mathbf{v} = (\mathbf{w} \times \mathbf{d})/|(\mathbf{w} \times \mathbf{d})| \tag{3}$$

A unit vector **n** is defined to complete the orthogonal bases also containing **v** and **w**:

$$\mathbf{u} = (\mathbf{v} \times \mathbf{w})/|\mathbf{v} \times \mathbf{w}| \tag{4}$$

The chip thickness $h(\phi,z)$, i.e., the thickness of the material removed by a flute, at any location on the cutter, can be determined as [17]:

$$h(\phi,z) = (v(\phi,z) \cdot n(\phi,z)) \sin\kappa / N \cdot \omega \tag{5}$$

$$v(\phi,z) = V\mathbf{d} + \omega \times r \tag{6}$$

where N is the number of teeth, ω is spindle speed, $v(\phi,z)$ is the cutter to stock relative velocity, not including spindle rotation, $n(\phi,z)$ is the cutter surface unit normal at tooth locating angle ϕ and axial location z, V is the velocity of the

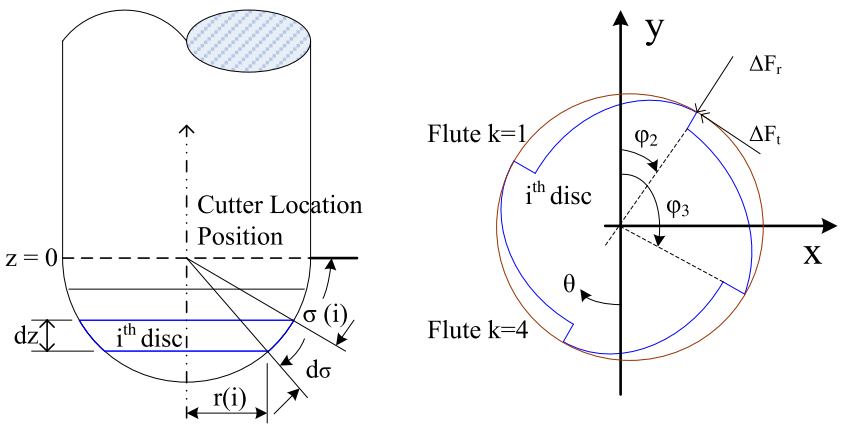

Fig. 7 Axial discretization of the ball end mill and force components estimation

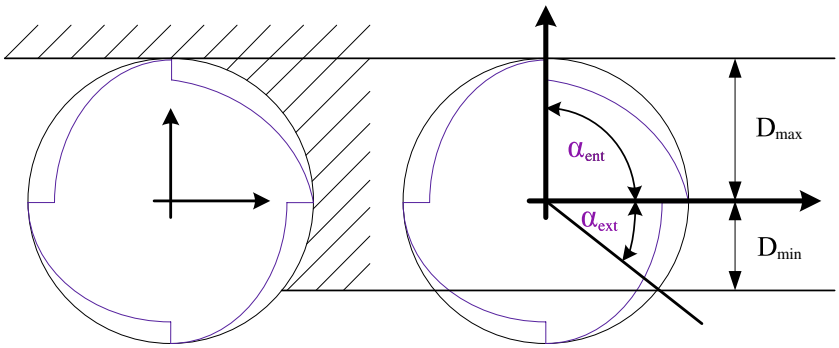

Fig. 8 Calculation of the entrance and exit angles for each disc

cutter center, and r is the locating vector from the cutter center to the point of interest on the cutter.

3.2 Model formulation of mechanistic forces

The envelope of the cutter is used in identifying the intersection of cutter and workpiece geometry, which is required in simulating the material removal process and in dynamically updating the blank geometry for graphical NC tool path verification.

The discrete mechanistic milling model can be used to estimate instantaneous force magnitude and direction [18]. It used a numerical technique which slices the cutter into a series of discs and sums the force contribution from each flute segment in the disc that is in contact with the workpiece.

For three axis machining $v(\phi,z)$ is uniform over the tool, but for five axis machining it varies depending on the relative components of the linear and angular velocity. The tooth force during cutting is directly proportional to the chip thickness. The different tangential (dF_t), radial (dF_r) and axial (dF_a) cutting forces acting on unit length of cutting edge are the following:

$$\begin{aligned} dF_t &= K_{tc}(h_a)^{-p_1}h(\phi,z)dz \\ dF_r &= K_{rc}(h_a)^{-p_2}h(\phi,z)dz \\ dF_a &= K_{ac}(h_a)^{-p_3}h(\phi,z)dz \end{aligned} \tag{7}$$

where K_{tc}, K_{rc}, K_{ac}, P_1, P_2 and P_3 are constants that depend on the workpiece material properties, tooth geometry, tool wear and material temperature, and h_a is the average chip thickness of the cut at some tool angle θ. The cutter is axially digitized with small disk elements with a uniform differential height of dz. The dynamic chip thickness is evaluated by subtracting the present coordinate of the cutting point from the previous surface generated by the preceding tooth [19]. Once the chip load is identified and cutting constants are evaluated for the local edge geometry, the cutting forces in Cartesian coordinate system can be evaluated as

$$\left[dF_{xyz}\right] = [T][dF_{rta}] \tag{8}$$

$$\begin{bmatrix} dF_x \\ dF_y \\ dF_z \end{bmatrix} = \begin{bmatrix} -\sin\phi\sin\kappa & -\cos\phi & -\sin\phi\cos\kappa \\ -\cos\phi\sin\kappa & \sin\phi & -\cos\phi\sin\kappa \\ -\cos\kappa & 0 & -\sin\kappa \end{bmatrix} \begin{bmatrix} dF_r \\ dF_t \\ dF_a \end{bmatrix} \tag{9}$$

The total cutting forces for the rotational position can be found integrating Eq. (10) along the axial depth of cut for all cutting flutes which are in contact with the workpiece.

$$\begin{aligned} F_x(\theta) &= \sum_{i=1}^{N} F_{xi}[\phi(z)] \\ F_y(\theta) &= \sum_{i=1}^{N} F_{yi}[\phi(z)] \\ F_z(\theta) &= \sum_{i=1}^{N} F_{zi}[\phi(z)] \end{aligned} \tag{10}$$

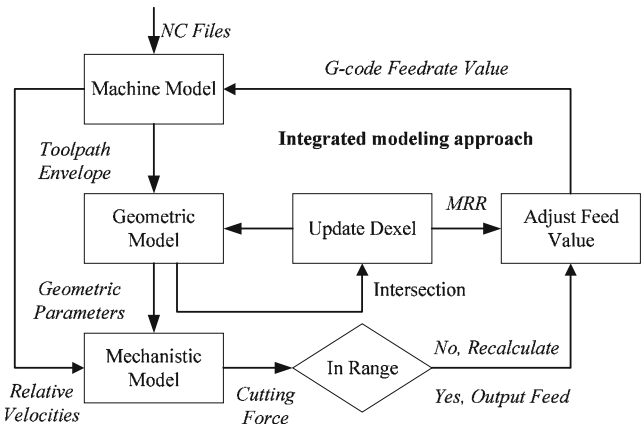

Fig. 9 Flowchart of the integrated modeling approach for feedrate scheduling

Table 1 Aluminum 6061 experiment conditions

Exp. No.	Spindle speed (rpm)	Feed (mm/min)	Radial depth (mm)	Type of radial cut	Axial depth (mm)
1	800	200	6.35	down milling	5.35
2	800	200	3.15	down milling	6.35
3	800	250	12.7	slot cut	4.62
4	800	300	6.32	up milling	3.32
5	1000	500	3.15	up milling	4.55
6	1000	800	5.35	down milling	7.66
7	1000	1000	8.55	down milling	5.85
8	1200	1200	10.5	down milling	10.2
9	1200	900	7.15	down milling	6.15
10	1200	700	5.35	down milling	8.82

$$
\begin{aligned}
F_x(\theta) &= \sum_{i=1}^{N} \int_{z_1}^{z_2} [-dF_{ri} \sin\phi_i \sin\kappa_i - dF_{ti} \cos\phi_i - dF_{ai} \sin\phi_i \cos\kappa_i] dz \\
F_y(\theta) &= \sum_{i=1}^{N} \int_{z_1}^{z_2} [-dF_{ri} \cos\phi_i \sin\kappa_i + dF_{ti} \sin\phi_i - dF_{ai} \cos\phi_i \cos\kappa_i] dz \\
F_z(\theta) &= \sum_{i=1}^{N} \int_{z_1}^{z_2} [-dF_{ri} \cos\phi_i - dF_{ai} \sin\kappa_i] dz
\end{aligned}
\tag{11}
$$

where N is the number of flutes on the cutter. z_1 and z_2 are the contact boundaries of the flute within the cut and can be found from the geometric model of each zone. The differential cutting forces are calculated along the full contact length for all flutes which are in cut, and digitally summed to find the total cutting forces $F_x(\theta)$, $F_y(\theta)$ and $F_z(\theta)$ at a given rotation angle. $\theta = \omega \cdot dt$ where ω is the spindle speed and dt is the differential time interval for digital integration. Only disc tooth elements engaged in the material, i.e., between the entrance and exit angles, are summed to find the forces.

4 Integrated model for feedrate scheduling

Generally, machining using end milling is classified into three steps: rough milling, semi-finish milling, and finish milling. In rough and semi-finish milling, machining time is the most important factor for better productivity. In finish milling, on the other hand, dimensional tolerance is the dominant factor. This paper presents a feedrate scheduling method for ball end milling that minimizes the machining time.

In the software developed during this research, the geometric and mechanistic models are executed in an integrated manner. Figure 9 shows the integrated modeling approach for feedrate scheduling. For each tool move contained in the NC part file, the toolpath envelope is checked for intersections with the dexel model, and the geometric model is updated accordingly. The entrance and exit angles, contact areas, are then calculated for each intersected axial disc from the intersection data, and stored. The mechanistic model is then used to estimate the feedrate necessary to maintain a desired force. This is an iterative process. First, the mechanistic model estimates the force produced by a "first guess" feedrate value. The feedrate is then adjusted, and the mechanistic model is invoked again. The iteration continues to within a given tolerance of a desired force value. This procedure is repeated for each tool move in the NC file, resulting in a set of optimal feedrates.

While the milling forces estimated by the mechanistic model are a function of chip thickness, it is possible for acceptable milling force values to be calculated while producing unacceptable chip thickness values. This case occurs particularly when a small amount of material is being removed [20]. In an effort to limit tool wear and flute damage caused by excessive chip loads, a user-defined maximum chip thickness value may be used. This method is actually quite similar to traditional methods where cutter feeds and speeds are selected from tabular data, the result of which is control of the maximum chip thickness produced, only in this case the maximum chip thickness is controlled for every tool move.

The feedrate optimization begins with an initial trial feedrate. The cutting force is calculated for this feedrate, and compared with the reference cutting force. If the difference is significant, a new trial feedrate is used to

Table 2 The calibration constants used for experiment prediction

Simulation conditions for ball end milling of free-form surface								
K_{TC}	K_{RC}	K_{AC}	P_1	P_2	P_3	Flutes	Discs	Helix angle
535	125	256	0.24	0.26	0.25	4	18	30°

calculated the cutting force, which is then compared with the reference cutting force again. The new trial feedrate can be calculated using Eq. 12 under the assumption that the feedrate has a linear relationship with the cutting force:

$$f_{next} = f_1 + (F_{ref} - F_1)(f_2 - f_1)/(F_2 - F_1) \quad (12)$$

where F_1 and F_2 are the maximum resultant cutting forces when the feedrates are f_1 and f_2 respectively, and F_{ref} is the reference resultant cutting force.

The calculation of the maximum chip thickness is a straightforward process. At each discrete rotational position, the chip thickness value of all engaged flute segments is required for force calculation. Therefore, the maximum chip thickness present during a given tool move may be obtained by storing the maximum value calculated. If the value during any given move is found to exceed the maximum allowable value, and the current force value is less than the upper bound on the acceptable force range, the feed iterations are exited. The output feed value is then adjusted to the value that produces the maximum allowable chip thickness. As there is a linear relationship between chip thickness and feedrate at any given location on the cutter, the required feed may be calculated using:

$$f_{out} = f_{current}(h_{desired}/h_{\max}) \quad (13)$$

f_{out} is the feed value output to the updated G-code file for the current move, $f_{current}$ is the current iteration feed value that resulted in excessive chip thickness, $h_{desired}$ is the user defined desired maximum chip thickness value, and $h_{\max}$ is the maximum chip thickness value calculated during the current tool move.

5 Simulation and experimental validation

Based on the extended dexel model of workpiece and STE, a prototype system of force prediction and feedrate selection was developed with Microsoft Visual C++ and OpenGL. In this system, the cutting force can be predicted along with simulation of the material removal process. Off-line feedrate scheduling regulates the maximum resultant cutting force during one revolution of a cutter at a reference value for a given NC code. The scheduling requires accurate predictions of the cutting force waveforms and profiles.

5.1 Application 1: prediction of cutting force

To validate this cutting force model, cutting forces were measured over a wide range of cutting conditions and compared with predicted values. Experiments were performed on a vertical machine tool. The workpiece material

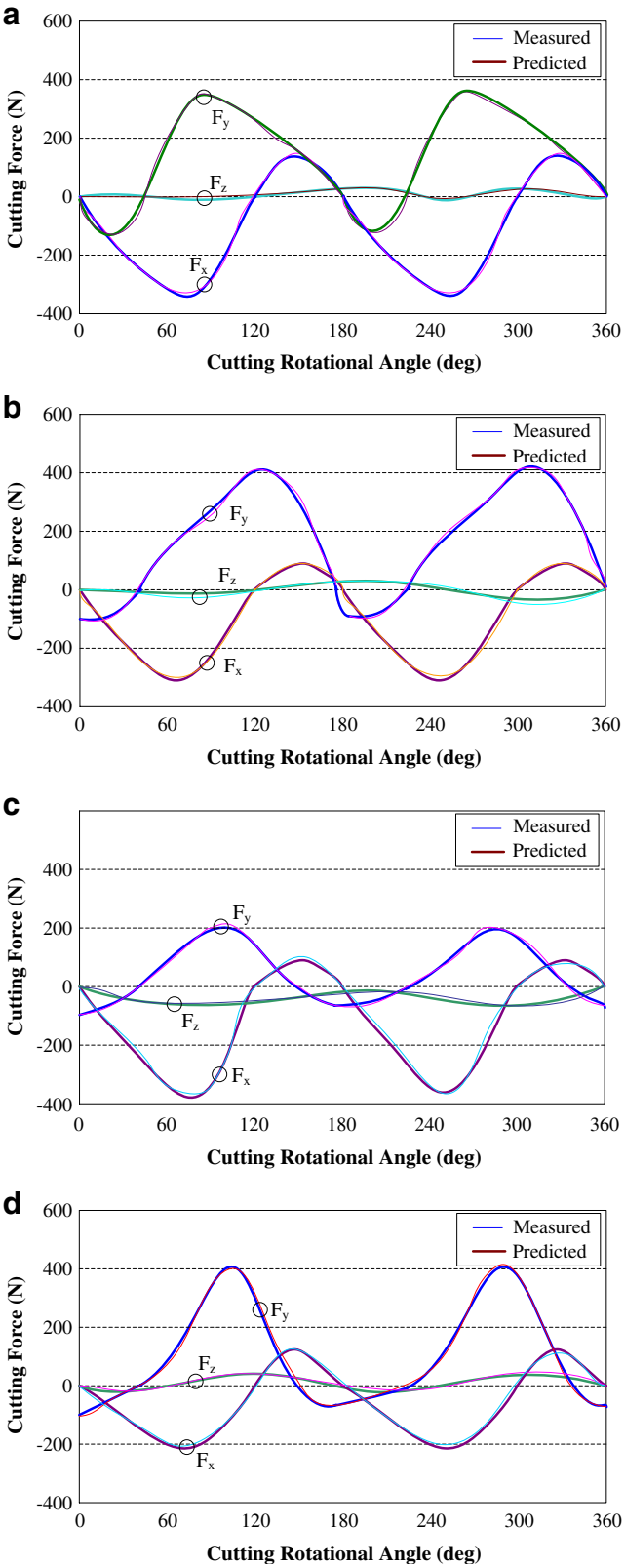

Fig. 10 Comparison of measured and predicted cutting forces for: (**a**) Exp.2, (**b**) Exp.3 (**c**) Exp.5, (**d**) Exp.7

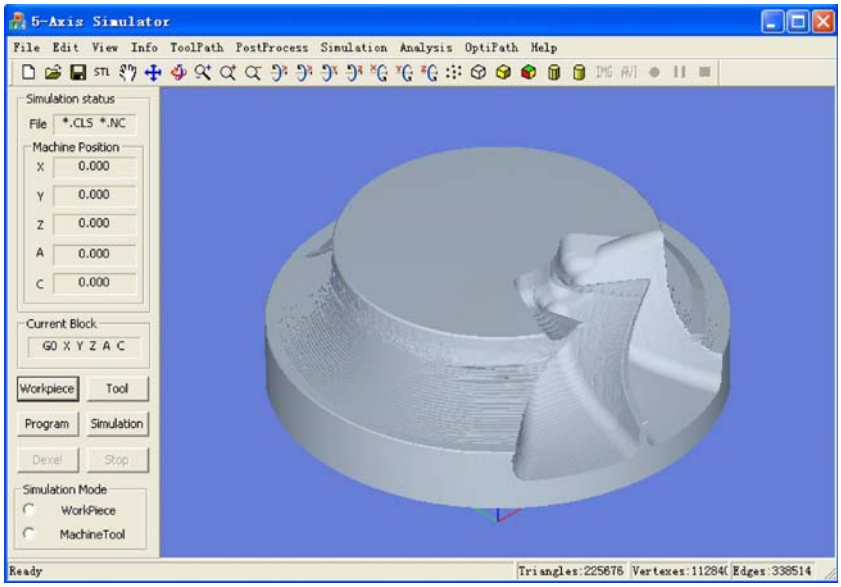

Fig. 11 Five-axis simulator interface and screenshot of impeller machining simulation

was Al 6061. All the tests were conducted with carbide ball-end mills with four flutes, a 30° helix angle, and a 10° rake angle. The 3D cutting forces were predicted using the determined cutting force coefficient parameters under various cutting conditions. Instantaneous three-dimensional cutting forces were measured by a tool dynamometer (Kislter, Dyn.9257A). The cutting conditions are presented in Table 1. The model is calibrated using the processed cut data from experiment in Table 1. The calibration constants used for these predictions are given in Table 2. Model simulation results are then compared to the other experiments to evaluate the force model over a range of cutting conditions. Figure 10 shows the measured and predicted cutting forces under four cutting conditions. As shown in the figure, the cutting forces were accurately predicted by the cutting force coefficients obtained from the experimental data. There is good agreement in both the magnitude and shape of the predicted and measured forces, with a maximum prediction error of 8%.

The main source for the force profile matching error is thought to be the rubbing forces, i.e., flank forces, at the edges of the cutter contacting the workpiece. When the

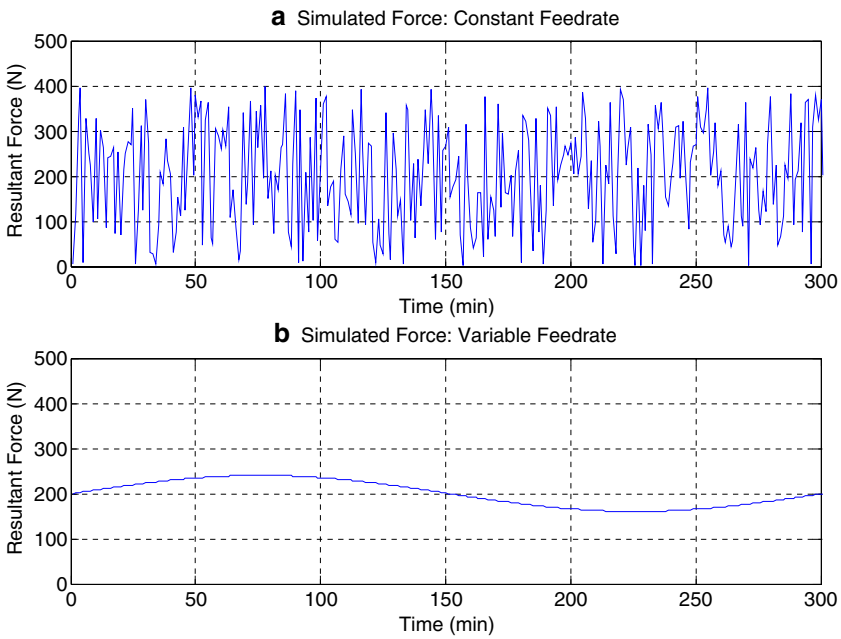

Fig. 12 Simulated forces during impeller machining using fixed and variable feeds. (**a**) Simulated Force: Constant Feedrate, (**b**) Simulated Force: Variable Feedrate

Table 3 Cutting and simulation conditions for impeller milling tests

Cutting conditions for impeller machining						
Cutting tool	Tool length	Spindle speed	Feedrate	Stock material	Mill time	Coolant
10 mm ball	45 mm	2500 rpm	720 mm/min	Aluminum	130 min 18 s	yes

uncut chip thickness is very small, or even zero, the corresponding edge forces are still significant.

5.2 Application 2: feedrate selection for impeller and propeller machining

Five-axis machining of a impeller blade provides an excellent example of surface variation. The impeller stock is made of aluminum and the cutting tool is a 10 mm ball end cutter. An NC program file generated by the UG NX4 was run through the simulation software. Figure 11 shows the screenshot of impeller machining simulation and five-axis simulator interface developed by the author. Figure 12 shows the force results for the simulation using a fixed feedrate of 800 mm/min and variable feeds. The variable feedrate was selected using the integrated model as shown in

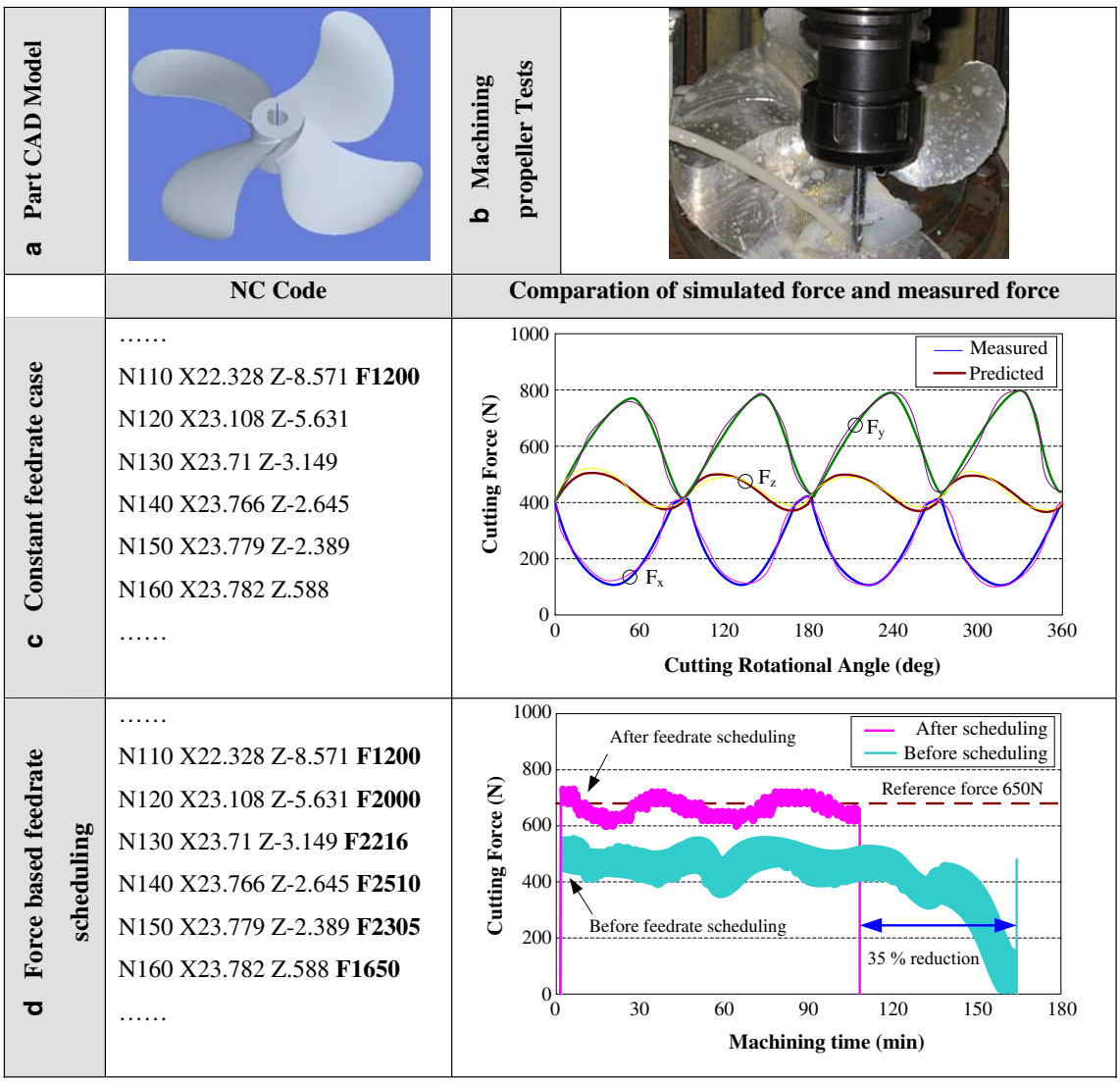

Fig. 13 Machining propeller part: (**a**) Part geometry, (**b**) Machining tests, (**c**) Comparison of simulated and measured forces (**d**) Comparison of force and process time before and after feedrate scheduling

Fig. 9. The conditions of the machining and simulation along with the required model constants are shown in Table 3.

Another propeller machining test was performed to validate the feedrate scheduling in Fig. 13(a,b). The cutting conditions for the propeller are the same as those given in Table 3 except for a spindle speed of 4000 rpm. The simulated and measured peak force for a constant feedrate of 1200 mm/min is shown in Fig. 13(c). Although the profiles are not an exact match, the magnitudes and trends of the direction forces are very similar between the estimated and measured force data. In addition to the use of approximate flute geometry, it is very difficult to get an exact match due to the finite accuracy inherent in the modeling. The feedrate scheduling was executed to regulate the cutting forces at a given level of 650N. The feedrate scheduling approach was applied to the part, and the optimal scheduling feedrate values were obtained in Fig. 13(d) for feedrate scheduling strategy. After generating the idea feedrate values, the force envelops before and after the feedrate scheduling were compared as shown in Fig. 13(d). As a result of feedrate scheduling, cutting forces were well regulated at the given reference cutting force within 15% variance. When the initial feedrate was 1200 mm/min, the machining time was reduced from 160 to 105 min, that is, reduced by 35%. The machining results showed that the cutting forces were readily regulated and controlled at the given level using the scheduled feedrates.

6 Conclusions

This work demonstrates the feasibility of combining a geometric model with a discrete mechanistic model for the purpose of five-axis force prediction and feedrate selection. The combined models of the software system are tied together in an integrated modeling approach, where the overall system is integrated such that the only links between components are passing data. Five-axis simulation results indicate that the integrated system model is capable of both prediction and selection. The proposed strategy was tested under various cutting conditions and when the integrated modeling approach based feedrate scheduling strategy was used, it was shown that the machining time can be decreased significantly along the tool path. Production time in propeller machining example was reduced considerably to 35% compared to constant feedrate cases.

Acknowledgements The authors acknowledge the financial support of National Natural Science Foundation of China (No. 50575138). Special thanks to Professor Robert B. Jerard for his generous help.

References

1. Lan TS, Hsu KS (2007) The implementation of optimum MRR on digital PC-based lathe system. Int J Adv Manufact Technol 35(3–4): 248–254
2. Li ZZ, Zheng M, Liu DC (2003) A solid model-based milling process simulation and optimization system integrated with CAD/CAM. J Mate Process Technol 138(1–3):513–517
3. Yazar Z, Koch KF, Altan T (1994) Feedrate optimization based on cutting force calculations in 3-axis milling of dies and molds with sculptured surfaces. Int J Mach Tool Manufact 34(3):365–377
4. Lim M, Hsiang MC (1997) Integrated planning for precision machining of complex surface. Int J Mach Tool Manufact 37:77–91
5. Baek DK, Ko TJ, Kim HS (2006) Chip volume prediction using a numerical control verification model. Int J Mach Tool Manufact 46(12–13):1326–1335
6. Liu XW, Cheng K (2005) Improved dynamic cutting force model in ball-end milling. Part I: theoretical modeling and experimental calibration. Int J Adv Manufact Technol 26(5):465–475
7. Taunsi N, Elbestawi MA (2003) Optimized feed scheduling in three axes machining. Part I: Fundamentals of the optimized feed scheduling strategy. Int J Mach Tool Manufact 43:253–267
8. Feng HY, Su N (2000) Integrated tool path and feedrate optimization for finishing machining of 3D plane surfaces. Int J Mach Tool Manufact 40:1557–1572
9. Li ZZ, Zhang ZH, Zheng L (2004) Feedrate optimization for variant milling process based on cutting force prediction. Int J Adv Manufact Technol 24(7–8):541–552
10. Ko JH, Cho DW (2004) Feedrate scheduling model considering transverse rupture strength of a tool for 3D ball-end milling. Int J Mach Tool Manufact 44:1070–1076
11. Erdim H, Lazoglu I, Ozturk B (2006) Feedrate scheduling strategies for free-form surfaces. Int J Mach Tool Manufact 46 (7–8):747–757
12. Guzel BU (2004) Increasing productivity in sculpture surface machining via off-line piecewise variable feedrate scheduling based on the force system model. Int J Mach Tool Manufact 44 (1):21–28
13. Li JG, Zhao H, Yao YX, Liu CQ (2007) Off-line optimization on NC machining based on virtual machining. Int J Adv Manufact Technol (in press). DOI 10.1007/s00170-006-0915-6
14. Ko JH, Cho DW (2004) Feedrate scheduling model considering transverse rupture strength of a tool for 3D ball-end milling. Int J Mach Tool Manufact 44:1070–1076
15. Jang D, Kim K, Jung J (2000) Voxel-based virtual multi-axis machining. Int J Adv Manufact Technol 16(10):709–713
16. Huang YC, Oliver JH (1994) NC milling error assessment and tool path correction. Comput Graphics Proc 28(4):287–294
17. Fussell BK, Jerard RB, Hemmett JG (2003) Modeling of cutting geometry and forces for 5-axis sculptured surface machining. Computer-Aided Des 35(4):333–346
18. Jerard RB (2006) Process simulation and feedrate selection for three-axis sculptured surface machining. Int J Manufact Res 2:136–156
19. Fussel BK, Jerard RB, Hemmett JG (2001) Robust feedrate selection for 3-axis NC machining using discrete models. J Manufact Sci Engin 123:214–224
20. Lee HU, Cho DW (2003) An intelligent feedrate scheduling based on virtual machining. Int J Adv Manufact Technol 22(11–12):873–882